Chaplygin gas halos

T. de Beer[a,b] and J.W. van Holten[c]

Lorentz Institute
Leiden University, Leiden NL
and
Nikhef, Amsterdam NL

Abstract

Unification of dark matter and dark energy as short- and long-range manifestations of a single cosmological substance is possible in models described by the generalized Chaplygin gas equation of state. We show it admits halo-like structures and discuss their density profiles, the resulting space-time geometry and the rotational velocity profiles expected in these models.

[a] *Present address:* Dept. of Physics, Univ. of Toronto, 60 St. George Str., Toronto, Canada
[b] *e-mail:* tdebeer@physics.utoronto.ca
[c] *e-mail:* vholten@nikhef.nl

1. Introduction

Careful measurements of the observable universe have shown that the list of ingredients contributing to the total energy density contains more than radiation, curvature and baryonic/standard-model matter [1, 2, 3, 4, 5, 6, 7, 8]. Assuming the theory of General Relativity to describe space-time geometry at astrophysical and cosmological length scales, it appears there are two more ingredients which behave qualitatively different, associated with dark matter and dark energy.

In the ΛCDM-model of cosmology dark matter is commonly associated with a cold gas of massive, electrically neutral non-relativistic particles of non-baryonic origin [9, 10, 11], whilst the dark energy is described by a cosmological constant which can be an infrared remnant of unknown fundamental physics [12, 13, 14, 15, 16]. However, although the associated length scales and qualitative behavior of dark matter and dark energy are different, there is no *a priori* reason to include two independent new components. Indeed it is possible to construct unified dark matter models (UDM) associating both dark components with a single unknown substance. Concrete examples of effective UDM theories are provided by models based on the equation of state of the *generalized Chaplygin gas* (gCg) [17, 18, 19, 20, 21, 22, 23, 24, 25, 26, 27, 28, 29, 30, 31, 32].

While it is well-known that the gCg can drive the observed accelerated expansion of the universe, see e.g. [24], to qualify as a dark-matter component as well it should be able to form dark-matter like halos in galaxies and galaxy clusters to explain the measured angular velocity distribution of stars in galaxies and the non-virial motion of galaxies in clusters. In this paper we address the question how to model spherical gCg halos and derive their short- and long-range properties to allow comparison with observational constraints on dark matter and dark energy; earlier work on these topics can be found in [26, 28, 29].

This paper is organized as follows. In section 2 we introduce the generalized Chaplygin gas as a fluid defined by a specific equation of state. We compute the speed of sound and derive a contraint imposed on the parameters in the gCg model by requiring it does not exceed the speed of light. We review the cosmological characteristics of a gCg in a homogeneous and isotropic Friedmann universe. In section 3 we address the possible existence of spherical halos of a gCg and show that their pressure and energy density profiles are governed by a modified form of the Tolmann-Oppenheimer-Volkov equation. Expressions for the long- and short-range radial structure of such halos are presented and discussed in section 4 and 5. Section 6 describes a modification of constraints in the presence of a de Sitter-like horizon to accomodate models in a wider range of parameter space; this is followed by a comparison with well-known CMB data in section 7. In section 8 we turn to the space-time geometry governed by a gCg-halo structure and derive an expression for the rotational velocity profile of test masses on circular orbits. In the final section 9 we summarize our results and draw conclusions from our analysis. Throughout this paper we use natural units in which $c = 1$.

2. The generalized Chaplygin gas

The generalized Chaplygin gas is characterized by the equation of state relating pressure p and energy density ε by

$$p = -A\varepsilon^{-\alpha}, \tag{1}$$

where A is a dimensionful proportionality constant and the exponent α is a positive number; the original Chaplygin gas model was defined with $\alpha = 1$ [33]. The equation of state can be converted to a relation between dimensionless quantities by defining a parameter μ with the dimensions of energy density such that $A = \mu^{1+\alpha}$, whence

$$\frac{p}{\mu} = -\left(\frac{\varepsilon}{\mu}\right)^{-\alpha}. \tag{2}$$

At constant entropy per particle the energy density and pressure are related to the number density of particles ρ by relations

$$\varepsilon = f(\rho), \qquad p = \rho f'(\rho) - f(\rho), \tag{3}$$

such that the pressure is the Legendre transform of the energy density with respect to density ρ. These conditions are solved by

$$\frac{\varepsilon}{\mu} = \left(1 + \left(\frac{\rho}{\rho_0}\right)^{1+\alpha}\right)^{1/(1+\alpha)}, \qquad \frac{p}{\mu} = -\left(1 + \left(\frac{\rho}{\rho_0}\right)^{1+\alpha}\right)^{-\alpha/(1+\alpha)}, \tag{4}$$

where ρ_0 is a constant of integration. From these relations one finds the adiabatic speed of sound c_s and the equation of state parameter w in the gCg to be given by [25]

$$c_s^2(\rho) = \frac{\partial p}{\partial \varepsilon} = \alpha \left(\frac{\varepsilon}{\mu}\right)^{-(1+\alpha)} = -\alpha w(\rho), \tag{5}$$

which is positive for any $\alpha > 0$.

In a space-time with metric $g_{\mu\nu}$ the energy-momentum tensor of a perfect fluid obeying the gCg equation of state takes the form

$$T^{\mu\nu} = pg^{\mu\nu} + (p + \varepsilon)\, u^\mu u^\nu, \tag{6}$$

where u^μ is the local 4-velocity of the fluid. It follows directly that in the limit of vanishing particle density $\rho = 0$ the energy-momentum tensor takes the form of a cosmological constant $\Lambda = \mu$:

$$\varepsilon = -p = \mu \quad \Rightarrow \quad T^{\mu\nu} = -\mu g^{\mu\nu}. \tag{7}$$

In contrast a dense gCg with $\rho \gg \rho_0$ behaves like a non-relativistic fluid:

$$\varepsilon \simeq \frac{\mu}{\rho_0}\rho, \qquad p \simeq 0, \tag{8}$$

which is the equation of state of a cold gas of non-relativistic particles with mass $m = \mu/\rho_0$. As a result the neutral gCg describes a substance which interpolates between dark matter in the dense early universe and dark energy in the dilute late universe.

This can be seen explicitly by considering a homogeneous gCg in a Friedmann-Lemaitre type universe with scale factor $a(t)$ and spatial curvature constant k:

$$ds^2 = -dt^2 + a^2 \left(\frac{dr^2}{1 - kr^2} + r^2 d\Omega^2 \right).$$ (9)

In this cosmological setting the covariant conservation of energy-momentum implies

$$\nabla_\mu T^{\mu\nu} = 0 \quad \Rightarrow \quad \frac{d(\varepsilon a^3)}{dt} + p \frac{da^3}{dt} = 0.$$ (10)

From this using the gCg equation of state one derives

$$\frac{\varepsilon}{\mu} = \left[1 + \left(\frac{a_0}{a} \right)^{3(1+\alpha)} \right]^{1/(1+\alpha)},$$ (11)

in agreement with equation (4) and ref. [23]. Clearly, for small $a \ll a_0$ the second term in the bracket dominates and $\varepsilon a^3 \simeq$ constant, whilst for large $a \gg a_0$ this term is negligible compared to unity and $\varepsilon \simeq \mu$. In fact for $\alpha \to 0$ the model reduces to a standard cosmological constant plus a non-relativistic gas like in the ΛCDM model:

$$\varepsilon \to \mu + \frac{m}{a^3}, \qquad m = \mu a_0^3.$$

Note that a universal bound $c_s^2 \leq 1$ in eq. (5) implies that, as at late times $\varepsilon/\mu \to 1$:

$$\alpha = c_s^2 \left(\frac{\varepsilon}{\mu} \right)^{1+\alpha} \leq 1.$$

3. Chaplygin gas halos

The existence of dark matter is not only suggested by cosmology; in fact the first clear evidence came from the average motion of galaxies in clusters [1] and from the motion of luminous baryonic matter in the outer regions of spiral galaxies [2, 3]. Assuming the mass distribution of galaxies to follow that of luminous matter, the rotation rate of stars far from the center of these galaxies violates Kepler's third law. This problem is solved if galaxies possess an extended halo of dark matter. Similar amounts of dark matter also explain the apparent non-virial motion of galaxies in clusters.

In the context of gCg models this implies that the equation of state (1) should allow for stable non-homogeneous self-gravitating density profiles. In this section we discuss conditions for the existence of spherically symmetric self-sustaining halos, neglecting the influence of baryonic components. That is, we use the Einstein equations with a source

3

term for a spherical non-homogeneous gCg profile to obtain an equation for halo structure. The starting point for our discussion is the following spherically symmetric *Ansatz* for the space-time metric

$$ds^2 = -\mathcal{A}(r)dt^2 + \mathcal{B}(r)dr^2 + r^2 d\Omega^2. \tag{12}$$

Taking the energy-momentum tensor of the gCg to be of the form (6) with non-trivial radial dependent pressure $p(r)$ and energy density $\varepsilon(r)$, the Einstein equations reduce to the set

$$\frac{1}{\mathcal{B}}\left[-\frac{1}{r^2} + \frac{\mathcal{B}}{r^2} + \frac{\mathcal{B}'}{\mathcal{B}r}\right] = 8\pi G\varepsilon,$$

$$\frac{1}{\mathcal{B}}\left[\frac{1}{r^2} - \frac{\mathcal{B}}{r^2} + \frac{\mathcal{A}'}{\mathcal{A}r}\right] = 8\pi G p, \tag{13}$$

$$\frac{1}{2\mathcal{B}}\left[\frac{\mathcal{A}''}{\mathcal{A}} - \frac{\mathcal{A}'}{2\mathcal{A}}\left(\frac{\mathcal{A}'}{\mathcal{A}} + \frac{\mathcal{B}'}{\mathcal{B}}\right) + \frac{1}{r}\left(\frac{\mathcal{A}'}{\mathcal{A}} - \frac{\mathcal{B}'}{\mathcal{B}}\right)\right] = 8\pi G p.$$

To solve the first equation we introduce a (non-covariant) mass function defined by summing the energy density in excess of μ up to radius r:

$$\mathcal{M}(r) = 4\pi \int_0^r dr'\, r'^2 \left(\varepsilon(r') - \mu\right). \tag{14}$$

Note that equation (4) guarantees that the integrand is always non-negative and therefore $\mathcal{M}$ increases monotonically with r from $\mathcal{M}(0) = 0$. The solution for $\mathcal{B}$ then takes the form

$$\mathcal{B}(r) = \left[1 - \frac{2G\mathcal{M}(r)}{r} - \frac{8\pi G\mu r^2}{3}\right]^{-1}. \tag{15}$$

This function has a singularity for $r = R$ such that

$$\frac{2G\mathcal{M}(R)}{R} = 1 - \frac{8\pi G\mu R^2}{3}. \tag{16}$$

The singularity at R exists as the right-hand side decreases monotonically as a function of R between $R = 0$ and $R = (3/8\pi G\mu)^{1/2}$, whilst on the same interval the left-hand side increases semi-monotonically starting from 0 as argued before:

$$\mathcal{M}' = 4\pi r^2 \left(\varepsilon(r) - \mu\right) \geq 0, \qquad 0 \leq r \leq \sqrt{\frac{3}{8\pi G\mu}}.$$

The singularity at R is to be interpreted as cosmic horizon similar to the cosmic horizon in de Sitter space for an observer located at the origin of co-ordinates.

To determine $\mathcal{M}(r)$ and $\mathcal{A}(r)$ we turn to the other two equations (13) implying the relations

$$-\frac{2p'}{\mu} = \frac{(p+\varepsilon)}{\mu}\frac{\mathcal{A}'}{\mathcal{A}} = \frac{2G}{r^2}\frac{(p+\varepsilon)}{\mu}\frac{\mathcal{M} + 4\pi r^3(p+\mu/3)}{1 - \frac{2G\mathcal{M}}{r} - \frac{8\pi G\mu r^2}{3}} \tag{17}$$

4

This is a modified (reparametrized) form of the Tolman-Oppenheimer-Volkov (TOV) equation applicable to the gCg. The original form of the equation was studied extensively in various parameter regimes in [26], which also established the existence of a singular radius R. In [29] the original TOV equation was similarly used to search for star-like solutions, which requires different boundary conditions however.

4. Halo profiles

We now turn to determining the characteristics of the solutions of our modified TOV equation for $\mathcal{M}(r)$, $\varepsilon(r)$ and $p(r)$. We specifically look for radially decreasing solutions of $\varepsilon(r)$ and $p(r)$ which are finite at the horizon $r = R$. The cosmological solution $\rho = 0$ such that $p + \varepsilon = 0$ and $p' = 0$ discussed in section 2 trivially satisfies the equation, but does not possess halo structure. Due to the non-linear nature of the equation non-trivial exact solutions are hard to find. In developing approximations we consider separately the regime of large r: $r \to R$ near the cosmic horizon; and small r: $r \to 0$ near the halo center. In the large-r regime it is convenient to introduce a dimensionless parameter x:

$$r = R(1 - x) \tag{18}$$

such that $r \to R$ implies $x \to 0$. We can then rewrite the TOV equation in the form

$$\left(1 - \frac{2G\mathcal{M}}{R(1-x)} - \frac{8\pi G\mu}{3} R^2 (1-x)^2\right) \frac{d}{dx} \frac{p}{\mu}$$

$$= 4\pi G\mu R^2 (1-x) \left(\frac{1}{3} + \frac{p}{\mu} + \frac{\mathcal{M}}{4\pi\mu R^3(1-x)^3}\right) \left(\frac{p}{\mu} + \frac{\varepsilon}{\mu}\right), \tag{19}$$

with

$$\frac{\varepsilon}{\mu} = 1 - \frac{1}{4\pi\mu R^3(1-x)^2} \frac{d\mathcal{M}}{dx}, \qquad \frac{p}{\mu} = -\left(\frac{\varepsilon}{\mu}\right)^{-\alpha}. \tag{20}$$

Large-r solutions are now constructed by power series in x:

$$\mathcal{M} = \sum_{n \geq 0} \frac{m_n}{n!} x^n, \qquad \varepsilon = \sum_{n \geq 0} \frac{\varepsilon_n}{n!} x^n, \qquad p = \sum_{n \geq 0} \frac{p_n}{n!} x^n. \tag{21}$$

Substitution into the equations (20) allows one to compute the coefficients to arbitrary order. Results for the first 4 coefficients in each expansion are collected in appendix A. To obtain these results equation (16) is used to relate $m_0 = \mathcal{M}(R)$ and R:

$$\frac{2Gm_0}{R} = 1 - \frac{8\pi G\mu}{3} R^2. \tag{22}$$

It is convenient to express all results in terms of two dimensionless variables characterizing the theory, the exponent α and

$$y = 8\pi G\mu R^2. \tag{23}$$

For the coefficients of the energy density we then get:

$$\frac{\varepsilon_0}{\mu} = y^{1/\alpha}, \qquad \frac{\varepsilon_1}{\mu} = \frac{1}{\alpha}\, y^{1/\alpha}\left(3 - y^{1+1/\alpha}\right),$$

$$\frac{\varepsilon_2}{\mu} = \frac{y^{1/\alpha}}{3\alpha^2}\left(\frac{3 - y^{1+1/\alpha}}{1 - y^{1+1/\alpha}}\right)\left[9 - 7\alpha - (19 + 8\alpha)y^{1+1/\alpha} + (6 + 3\alpha)y^{2+2/\alpha}\right],$$

$$\frac{\varepsilon_3}{\mu} = \frac{y^{1/\alpha}}{15\alpha^3\left(1 - y^{1+1/\alpha}\right)}\left[-405 + 945\alpha - 630\alpha^2 + \left(2517 - 282\alpha + 30\alpha^2\right)y^{1+1/\alpha}\right. \tag{24}$$

$$- \left(4215 + 3035\alpha + 660\alpha^2\right)y^{2+2/\alpha} + \left(2839 + 2937\alpha + 780\alpha^2\right)y^{3+3/\alpha}$$

$$\left. - \left(836 + 958\alpha + 270\alpha^2\right)y^{4+4/\alpha} + \left(90 + 105\alpha + 30\alpha^2\right)y^{5+5/\alpha}\right],$$

Observe, that for the energy density to decrease with distance we must require $\varepsilon_1 \geq 0$ or

$$y^{1+1/\alpha} \leq 3.$$

The corresponding coefficients of the pressure are

$$\frac{p_0}{\mu} = -\frac{1}{y}, \qquad \frac{p_1}{\mu} = \frac{1}{y}\left(3 - y^{1+1/\alpha}\right),$$

$$\frac{p_2}{\mu} = \frac{1}{3\alpha y}\left(\frac{3 - y^{1+1/\alpha}}{1 - y^{1+1/\alpha}}\right)\left[-16\alpha - (7 - 4\alpha)y^{1+1/\alpha} + 3y^{2+2/\alpha}\right],$$

$$\frac{p_3}{\mu} = \frac{1}{15\alpha^2 y\left(1 - y^{1+1/\alpha}\right)}\left[-1980\alpha^2 + \left(351 - 732\alpha + 1740\alpha^2\right)y^{1+1/\alpha}\right. \tag{25}$$

$$- \left(885 - 415\alpha + 540\alpha^2\right)y^{2+2/\alpha} + \left(739 + 117\alpha + 60\alpha^2\right)y^{3+3/\alpha}$$

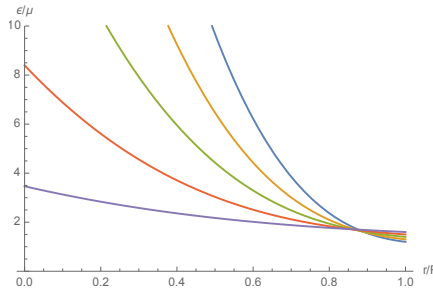$$\left. - (251 + 103\alpha)y^{4+4/\alpha} + (30 + 15\alpha)y^{5+5/\alpha}\right].$$

Fig. 4.1: ε/μ to order x^3 vs. r/R for $\alpha = 1$
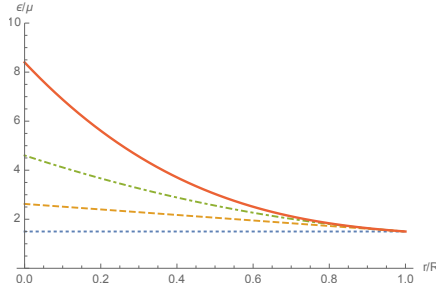and from right to left: $y = (1.2, 1.3, 1.4, 1.5, 1.6)$.

6

Fig. 4.2: ε/μ vs. r/R for $\alpha = 1$ and $y = 1.5$ to order x^n
with from bottom to top $n = (0, 1, 2, 3)$.

In figure 4.1 we show the results for the energy density ε/μ as a function of r/R to 3rd order in x for the value $\alpha = 1$ and various values of y. Similar figures for smaller values of α are collected in appendix B. For the curve with $\alpha = 1$ and $y = 1.5$ we also show separately the 0th-, 1st-, 2nd- and 3rd-order result for ε/μ in figure 4.2. For this case the results are seen to converge well in the domain of large-r.

5. Newtonian regime

In the small-r regime we can find a solution of the modified TOV equation using the newtonian approximation [28], in which it is assumed that $|p| \ll \mu \ll \varepsilon$ and

$$\frac{2G\mathcal{M}}{r} \ll 1, \quad \text{whilst} \quad \frac{\mathcal{M}}{4\pi\mu r^3} \gg 1. \tag{26}$$

Thus close to the center of the halo $\mathcal{M}$ is to grow faster than r and slower than r^3 with increasing distance. In this approximation the modified TOV equation reduces to the condition for newtonian hydrostatic equilibrium:

$$\frac{p'}{\varepsilon} = -\frac{G\mathcal{M}}{r^2}. \tag{27}$$

Using the gCg equation of state it follows that

$$G\mathcal{M} = \frac{\alpha r^2}{1+\alpha} \frac{d}{dr} \left[\left(\frac{\varepsilon}{\mu} \right)^{-(1+\alpha)} \right]. \tag{28}$$

Differentiating once more with respect to r this results in a differential equation for the energy density:

$$G\mathcal{M}' \simeq 4\pi G r^2 \varepsilon = \frac{\alpha}{1+\alpha} \frac{d}{dr} \left\{ r^2 \frac{d}{dr} \left[\left(\frac{\varepsilon}{\mu} \right)^{-(1+\alpha)} \right] \right\}, \tag{29}$$

with the solution

$$\frac{\varepsilon}{\mu} = \left(\frac{r}{r_c} \right)^{-2/(2+\alpha)}, \qquad 2\pi G\mu r_c^2 = \frac{\alpha(4+3\alpha)}{(2+\alpha)^2}. \tag{30}$$

7

For the effective mass function this implies

$$\frac{G\mathcal{M}(r)}{r_c} = \frac{\alpha(4+3\alpha)}{(1+\alpha)(2+\alpha)} \left(\frac{r}{r_c}\right)^{(4+3\alpha)/(2+\alpha)}, \tag{31}$$

which satifies the initial assumptions (26) for all positive values of α. Indeed, in the limit $\alpha \to 0$ it is seen to grow as r^2, whilst in the limit $\alpha \to \infty$ it grows as r^3. Finally the assumption of small pressure: $|p| \ll \mu$, is satisfied in the domain $r \ll r_c$, with $|p| = 0$ in the center where the energy density ε diverges, although the mass function $\mathcal{M}$ vanishes there and remains finite for all r in the newtonian regime.

In terms of the parameter y introduced in (23) the expression (30) for the energy density can be recast in the form

$$\frac{\varepsilon}{\mu} = \left(\frac{r}{R}\right)^{-2/(2+\alpha)} \left[\frac{(2+\alpha)^2 y}{4\alpha(4+3\alpha)}\right]^{-1/(2+\alpha)}. \tag{32}$$

In figure 5.1 this expression is plotted and compared with the large-r expansion for the cases $\alpha = 1$ and three values of y.
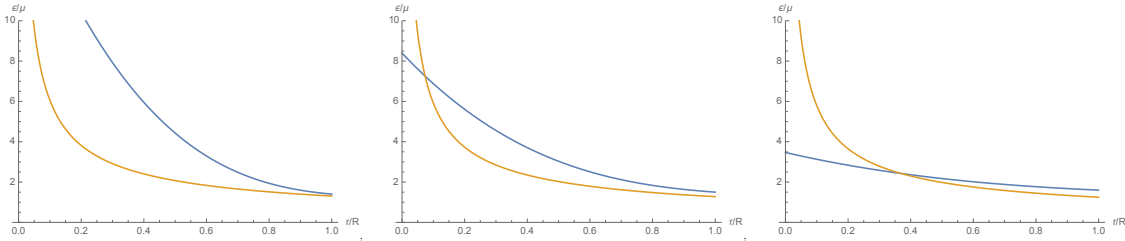

Fig. 5.1: Newtonian approximation (steeper orange curve) vs. large r-expansion (flatter blue curve) of ε/μ to order x^3 for $\alpha = 1$ and $y = 1.4$ (left), $y = 1.5$ (middle) and $y = 1.6$ (right).

These figures show that agreement between the two approximations in the large-r region is quite good, especially for the lowest value of y; this can be explained as

$$\left(\frac{r_c}{R}\right)^2 = \frac{4\alpha(4+3\alpha)}{(2+\alpha)^2 y},$$

and this ratio is close to 2 for the values of α and y used in the plots. For these and similar parameter values the whole region inside the horizon $r \leq R$ is inside the domain of the newtonian approximation, and it should get better the smaller the values of y. The figures also show that the large-r expansion overestimates the small-r values for the smaller value of y, while underestimating them for the larger y value. The same tendencies hold for lower values of α, although the range of validity of the large-r expansion is considerably more restricted there, as shown in appendix B.

8

6. Models with $\alpha > 1$

So far we have considered models with $\alpha \leq 1$ on the assumption that there is a universal bound on the speed of sound $c_s^2 \leq 1$. However, such a bound may be too strong in the presence of a horizon. In fact for a radially decreasing energy density in the domain $r \leq R$ equation (5) only requires

$$\alpha \leq \frac{\alpha}{c_s^2(R)} = \left(\frac{\varepsilon_0}{\mu}\right)^{1+\alpha} = y^{1+1/\alpha}. \tag{33}$$

A natural boundary condition is to let c_s take its maximal value on the horizon: $c_s(R) = 1$, which happens if the parameters α and y are related by

$$\alpha = y^{1+1/\alpha}. \tag{34}$$

As the asymptotic energy density $\varepsilon_0/\mu = y^{1/\alpha} > 1$ it follows that in this case also $\alpha > 1$.
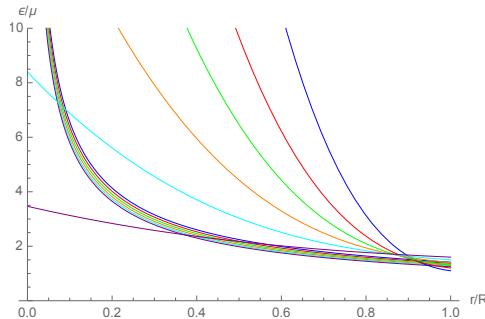

Fig. 6.1: Radial profile of the energy density ε/μ for $c_s(R) = 1$ in the 3rd-order large-r and newtonian approximations; from right to left $\alpha = (1.2, 1.4, 1.6, 1.8, 2.0)$.

In fig. 6.1 we have plotted the energy density profiles for these models taking values of α ranging from 1.2 to 2.0. The narrow bundle of lines represents the newtonian approximations, the wider bundle of lines with the lower asymptotic values of ε_0/μ represents the large-r approximations, which are relevant for r-values close to R. Even there the newtonian regime seems to be close to the true solution, which can be traced to the fact that in all these cases $R < r_c$, the more so for larger values of α. The exact asymptotic values of ε_0/μ in the figure are all in the range 1.08 - 1.26, close to unity.

7. Cosmological inference

Having worked out halo profiles predicted by gCg models, we can actually take input from cosmological data on dark matter and dark energy to fix some parameters. The parameter ε_0 is the total asymptotic energy density near the de Sitter horizon. It is composed of both a dark-matter and a dark-energy like component. We first have to determine how to

separate these components for the gCg cosmology discussed here. Consider the spatial line element at fixed t:

$$ds^2 = \frac{dr^2}{1 - \frac{2G\mathcal{M}}{r} - \frac{8\pi G\mu}{3} r^2} + r^2 d\Omega^2. \tag{35}$$

Asymptotically this behaves like the Schwarzschild-de Sitter line element at fixed t, with $\mathcal{M}(R) = m_0$ the mass inside the sphere within the horizon, and μ the asymptotic cosmological constant. This suggests we interpret the asymptotic energy density ε_0 as composed of a dark matter and a dark energy component such that

$$\frac{\varepsilon_{de\,0}}{\mu} = 1, \qquad \frac{\varepsilon_{dm\,0}}{\mu} = y^{1/\alpha} - 1. \tag{36}$$

Observations of the CMB [8] give the ratio in the early universe to be

$$\frac{\varepsilon_{dm}}{\varepsilon_{de}} = 0.39. \tag{37}$$

Associating this value to our asymptotic expressions we get

$$y = (1.39)^\alpha. \tag{38}$$

Thus y varies between $y = 1$ for $\alpha = 0$ to $y = 1.39$ for $\alpha = 1$. These results are in the range previously considered. It appears that the results for values $\alpha > 1$ do not fit the relation (34) very well.
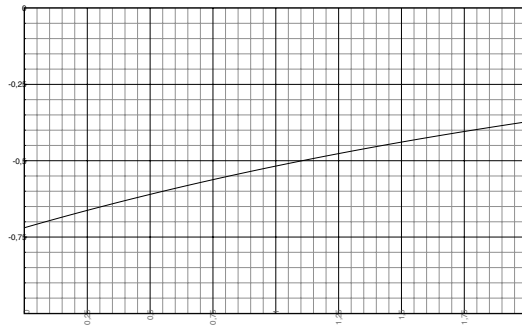

Fig. 7.1: w_0 vs. α for the estimated asymptotic dark matter and energy densities inferred from CMB data.

Similarly we can determine the asymptotic equation of state parameter for the gCg:

$$w_0 = -\frac{1}{y^{1+1/\alpha}}, \tag{39}$$

with values between $w_0 = -0.72$ for $\alpha = 0$ and $w_0 = -0.52$ for $\alpha = 1$, as shown in fig. 7.1. Note that some strong upper limits on α were suggested in refs. [20, 27, 30], but these seem difficult to reconcile with the large-r results (24).

10

8. Space-time geometry and rotation profiles

The space-time geometry in the spherically symmetric gCg halo is that of the line element (12), where $\mathcal{B}(r)$ is given by (15) and $\mathcal{A}(r)$ is the solution of equation (17):

$$\mathcal{A}(r) = \left[1 - \left(\frac{\varepsilon}{\mu}\right)^{-(1+\alpha)}\right]^{\frac{-2\alpha}{1+\alpha}}, \tag{40}$$

where the constant of integration has been fixed so that $\mathcal{A}(0) = 1$. With this choice the space-time is flat in the center of the halo. The line element (12) implies for light-like radial geodesics

$$\left(\frac{dr}{dt}\right)^2 = \mathcal{A}(r)\mathcal{B}^{-1}(r) \overset{r=R}{\longrightarrow} 0, \tag{41}$$

showing explicitly the existence of the horizon at R such that $\mathcal{B}^{-1}(R) = 0$. In the newtonian regime the expressions take the approximate form

$$\mathcal{A}_{newt} = \left[1 - \left(\frac{r}{r_c}\right)^{\frac{2+2\alpha}{2+\alpha}}\right]^{\frac{-2\alpha}{1+\alpha}},$$

$$\mathcal{B}_{newt} = \left[1 - \frac{2\alpha(4+3\alpha)}{(1+\alpha)(2+\alpha)}\left(\frac{r}{r_c}\right)^{\frac{2+2\alpha}{2+\alpha}} - \frac{4\alpha(4+3\alpha)}{3(2+\alpha)^2}\left(\frac{r}{r_c}\right)^2\right]^{-1}. \tag{42}$$

Note the limits

$$\alpha = 0: \quad \mathcal{A}_{newt} = \mathcal{B}_{newt} = 1,$$

$$\alpha = 1: \quad \mathcal{A}_{newt} = \left[1 - \left(\frac{r}{r_c}\right)^{4/3}\right]^{-1}, \quad \mathcal{B}_{newt} = \left[1 - \frac{7}{3}\left(\frac{r}{r_c}\right)^{4/3} - \frac{28}{27}\left(\frac{r}{r_c}\right)^2\right]^{-1}. \tag{43}$$

Geodesic orbits for testmasses m in a spherically symmetric space-time (12) are planar, which we will take to be the equatiorial plane $\theta = \pi/2$. In addition they are characterized by two constants of motion: the specific energy $\eta = E/m$ determined by the time dilation factor

$$\eta = \mathcal{A}\frac{dt}{d\tau}, \tag{44}$$

and the specific angular momentum $\ell = L/m$ determined by the rotational velocity

$$\ell = r^2 \frac{d\varphi}{d\tau}. \tag{45}$$

Finally time-like line elements satisfy the hamiltonian constraint

$$\mathcal{A}\left(\frac{dt}{d\tau}\right)^2 = 1 + \mathcal{B}\left(\frac{dr}{d\tau}\right)^2 + r^2\left(\frac{d\varphi}{d\tau}\right)^2.$$

11

In view of the preceeding results, for circular orbits with constant $r = \mathsf{r}_*$ this implies the relation

$$\eta^2 = \mathcal{A}(\mathsf{r}_*)\left(1 + \frac{\ell^2}{\mathsf{r}_*^2}\right), \tag{46}$$

whilst the stability of such orbits requires vanishing radial acceleration:

$$\left.\frac{d^2r}{d\tau^2}\right|_{r=\mathsf{r}_*} = 0 \quad\Rightarrow\quad \frac{\ell^2}{\mathsf{r}_*^2} = \left[\frac{-2\alpha r\frac{\varepsilon'}{\mu}}{\frac{\varepsilon}{\mu}\left(\left(\frac{\varepsilon}{\mu}\right)^{1+\alpha} - 1\right) + \alpha r\frac{\varepsilon'}{\mu}}\right]_{r=\mathsf{r}_*}. \tag{47}$$

In the newtonian regime $\mathsf{r}_* < r_c$, cf. (30), this becomes

$$v^2(\mathsf{r}_*) = \frac{\ell^2}{\mathsf{r}_*^2} = \frac{4\alpha\left(\frac{\mathsf{r}_*}{r_c}\right)^{\frac{2+2\alpha}{2+\alpha}}}{(2+\alpha) - (2+3\alpha)\left(\frac{\mathsf{r}_*}{r_c}\right)^{\frac{2+2\alpha}{2+\alpha}}}, \tag{48}$$

where $v(\mathsf{r}_*)$ is the orbital velocity. For example for $\alpha = 1$, which is in the regime $\mathsf{r}_* < r_c$ all the way up to the horizon R, we get

$$v^2(\mathsf{r}_*) = \frac{4}{3}\left(\frac{\mathsf{r}_*}{r_c}\right)^{4/3}\frac{1}{1 - \frac{5}{3}\left(\frac{\mathsf{r}_*}{r_c}\right)^{4/3}} \simeq \frac{4}{3}\left(\frac{\mathsf{r}_*}{r_c}\right)^{4/3}\left(1 + \frac{5}{3}\left(\frac{\mathsf{r}_*}{r_c}\right)^{4/3} + ...\right). \tag{49}$$

To lowest-order approximation it follows that

$$v(\mathsf{r}_*) = \frac{2}{\sqrt{3}}\left(\frac{\mathsf{r}_*}{r_c}\right)^{2/3}. \tag{50}$$

In this discussion we have implicitly assumed that the space-time described by the line element (40) is stationary. However the existence of the horizon at $r = R$ where $\mathcal{B}^{-1}(R) = 0$ and the related homogeneous cosmological space-times (9) indicate a time-dependent expanding geometry. We can make this explicit by performing a co-ordinate transformation defined implicitly by two functions $G(r)$ and $K(r)$ which are solutions of the equations

$$G = \sqrt{\mathcal{A} + H^2r^2}, \qquad \frac{rK_r}{K} = 1 - \sqrt{\frac{\mathcal{A}\mathcal{B}}{\mathcal{A} + H^2r^2}}, \tag{51}$$

where $K_r = dK/dr$ and H is the asymptotic Hubble constant

$$H = \sqrt{\frac{8\pi G\mu}{3}}. \tag{52}$$

Introducing new time and radial co-ordinates τ and ϱ:

$$d\tau = dt - \frac{Hr(1 - rK_r/K)}{G^2 - H^2r^2}dr, \qquad \varrho = e^{-H\tau}\frac{K(r)}{r}, \tag{53}$$

12

the line-element (40) takes the form

$$ds^2 = -\gamma^2(\varrho,\tau)d\tau^2 + e^{2H\tau}\kappa^2(\varrho,\tau))\left(d\varrho^2 + \varrho^2 d\Omega^2\right),\tag{54}$$

where γ and κ are given in terms of the solutions of eqs. (51) as

$$\gamma(\varrho,\tau) = G(r), \qquad \kappa(\varrho,\tau) = K(r).\tag{55}$$

This shows that γ and κ are in fact functions of a single variable $e^{H\tau}\varrho = K(r)/r$. Equation (54) is to replace relation (9) when taking a simple form of halo structure of dark matter into account. It also follows that orbits $r = \mathsf{r}_*$ are near-closed circular only in the newtonian limit where the period $T = 2\pi \mathsf{r}_*/v(\mathsf{r}_*)$ of the orbit is much smaller than the asymptotic Hubble time $1/H$.

9. Summary and discussion

In this paper we have analysed the structure and cosmological implications of spherical halos of a generalized Chaplygin gas. We have shown that a non-trivial spherically symmetric distribution of gCg creates a horizon at finite radial co-ordinate (but infinite proper distance) in agreement with [26]. The density of the gas decreases monotonically towards the horizon, but remains finite non-zero up to the largest distances. We have also found that in many cases the newtonian approximation for the structure of the halo works well, even though the space-time itself is characterized by a non-flat metric with coefficients (42). It gives rise to a rather weak dependence on the radius of orbital velocities of test masses in circular orbits, equation (48), for orbits much smaller than the horizon distance.

For a realistic description of cosmological structures the model has to be extended in several ways. First, the observable universe contains a large number of clusters of galaxies with overlapping dark-matter halos within a single de Sitter-like horizon. Still, these would be expected to give rise to a universal asymptotic behaviour as described by our large-r expansion in section 4. Second, in addition to dark matter and dark energy our universe also contains baryonic matter and radiative components; it may also contain additional dark-matter components. All of these have to be taken into account to get a realistic cosmology as discussed e.g. in [23, 25].

Nevertheless taking into account such simplifications made here the generalized Chaplygin gas appears to offer a more flexible effective theory of dark energy and dark matter allowing for richer structures with varying dark matter as well as dark energy density than a simple cosmological constant, as in the ΛCDM models. As such it can be of value in parametrizing the observed cosmological features of our universe.

Appendix A

The expansion coefficients in equations (21) are related by the definition of $\mathcal{M}$, equation (14), and the gCg equation of state (2). As a result

$$\frac{\varepsilon_0}{\mu} = 1 - \frac{m_1}{4\pi\mu R^3}, \qquad \frac{\varepsilon_1}{\mu} = -\frac{m_2 + 2m_1}{4\pi\mu R^3},$$

$$\frac{\varepsilon_2}{\mu} = -\frac{m_3 + 4m_2 + 6m_1}{4\pi\mu R^3}, \quad \frac{\varepsilon_3}{\mu} = -\frac{m_4 + 6m_3 + 18m_2 + 24m_1}{4\pi\mu R^3}, \tag{56}$$

and

$$\frac{p_0}{\mu} = -\left(\frac{\varepsilon_0}{\mu}\right)^{-\alpha}, \qquad \frac{p_1}{\mu} = \alpha\left(\frac{\varepsilon_0}{\mu}\right)^{-(1+\alpha)}\frac{\varepsilon_1}{\mu},$$

$$\frac{p_2}{\mu} = \alpha\left(\frac{\varepsilon_0}{\mu}\right)^{-(1+\alpha)}\frac{\varepsilon_2}{\mu} - \alpha\left(1+\alpha\right)\left(\frac{\varepsilon_0}{\mu}\right)^{-(2+\alpha)}\left(\frac{\varepsilon_1}{\mu}\right)^2,$$

$$\frac{p_3}{\mu} = \alpha\left(\frac{\varepsilon_0}{\mu}\right)^{-(1+\alpha)}\frac{\varepsilon_3}{\mu} - 3\left(1+\alpha\right)\left(\frac{\varepsilon_0}{\mu}\right)^{-(2+\alpha)}\frac{\varepsilon_1\varepsilon_2}{\mu^2}$$

$$+ \alpha\left(1+\alpha\right)\left(2+\alpha\right)\left(\frac{\varepsilon_0}{\mu}\right)^{-(3+\alpha)}\left(\frac{\varepsilon_1}{\mu}\right)^3. \tag{57}$$

Using these results in the modified TOV equation (19) we get in terms of $y = 8\pi G\mu R^2$

$$\frac{2Gm_0}{R} = 1 - \frac{y}{3}, \qquad \frac{2Gm_1}{R} = y - y^{1+1/\alpha},$$

$$\frac{2Gm_2}{R} = -2y + \left(2 - \frac{3}{\alpha}\right)y^{1+1/\alpha} + \frac{1}{\alpha}y^{2+2/\alpha},$$

$$\frac{2Gm_3}{R} = 2y\left(1 - y^{1+1/\alpha}\right)$$

$$-\frac{1}{3\alpha^2}\left(\frac{3 - y^{1+1/\alpha}}{1 - y^{1+1/\alpha}}\right)\left[(9 - 19\alpha)\,y^{1+1/\alpha} - (19 + 20\alpha)\,y^{2+2/\alpha} + (6 + 3\alpha)\,y^{3+3/\alpha}\right] \tag{58}$$

14

Appendix B

Here we show the 3rd-order large-r expansion of the energy density ε/μ as a function of r/R for values of the Chaplygin exponent $\alpha = (0.8, 0.6, 0.4)$. For the smallest values of α the expansion seems to be reliable only at the very high end of r-values.
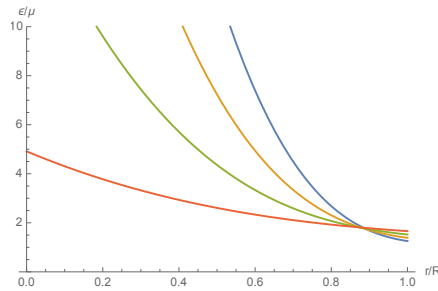

Fig. B.1: ε/μ vs. r/R for $\alpha = 0.8$ and from right to left $y = (1.2, 1.3, 1.4, 1.5)$.
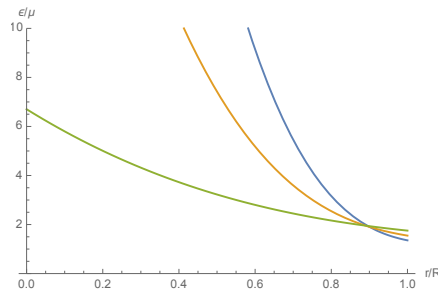

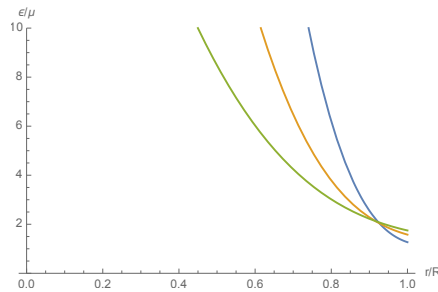Fig. B.2: ε/μ vs. r/R for $\alpha = 0.6$ and from right to left $y = (1.2, 1.3, 1.4)$.

Fig. B.3: ε/μ vs. r/R for $\alpha = 0.4$ and from right to left $y = (1.1, 1.2, 1.25)$.

We also show the comparison of the large-r expansion with the newtonian approximation for the energy density for the very small value $\alpha = 0.25$ and two values of y for which $r_c < R$.
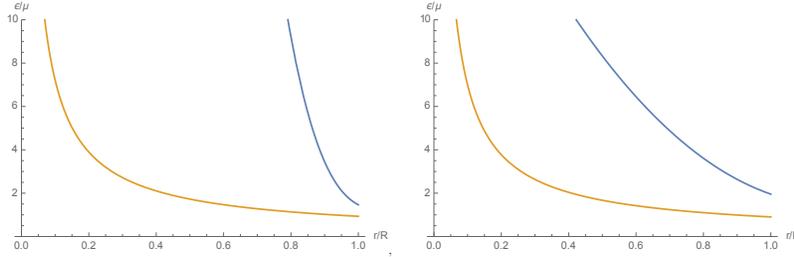
15

Fig. B.4 Comparison of newtonian approximation (lower curve) vs. large-r expansion (upper curve) for $\alpha = 0.25$ and $y = 1.1$ (left), $y = 1.1825$ (right).

In both cases the newtonian approximation underestimates the large-r value of the energy density, the more so for larger y, whereas the large-r expansion diverges much too fast for values of r away from the horizon $r = R$.

References

[1] F. Zwicky, "Die rotverschiebung von extragalaktischen nebeln," *Helvetica Physica Acta* **6** (1933) 110.

[2] A. Bosma and P.C. van der Kruit, "The local mass-to-light ratio in spiral galaxies," *Astron. Astrophys.* **79** (1979) 281–286.

[3] V. C. Rubin, N. Thonnard, and J. Ford, W. K., "Rotational properties of 21 SC galaxies with a large range of luminosities and radii, from NGC 4605 /R = 4kpc/ to UGC 2885 /R = 122 kpc/," *Astrophys. J.* **238** (1980) 471.

[4] D. Clowe et al., "A direct empirical proof of the existence of dark matter," *Astrophys.J.* **648** (2006) L109–L113, arXiv:astro-ph/0608407.

[5] A.G. Riess et al., "Observational Evidence from Supernovae for an Accelerating Universe and a Cosmological Constant," arXiv:astro-ph/9805201.

[6] S. Perlmutter, "Measurements of Omega and Lambda From 42 High-Redshift Supernovae," *Astrophys. J.* **517** (1999) 565–586, arXiv:astro-ph/9812133.

[7] P. Astier and R. Pain, "Observational evidence of the accelerated expansion of the universe," *Comptes Rendus Phys.* **13** (2012) no. 6-7, 521–538, arXiv:1204.5493 [astro-ph].

[8] P. Ade et al., "Planck 2015 results," *Astron. Astrophys.* **594** (2016) A13, arXiv:1502.01589 [astro-ph].

[9] G. Steigman and M.S. Turner, "Cosmological constraints on the properties of weakly interacting massive particles," *Nucl. Phys.* **B253** (1985) 375.

[10] A.H.G. Peter, "Dark Matter: A Brief Review," Proc. Frank N. Bash Symposium (2011) , `arXiv:1201.3942 [astro-ph]`.

[11] A. Ringwald, "Alternative dark matter candidates: Axions," `arXiv:1612.08933 [hep-ph]`.

[12] C. Wetterich, "Cosmology and the fate of dilatation symmetry," *Nucl. Phys. B* **302** (1988) 668–696.

[13] C. Wetterich, "Quintessence - the dark energy in the universe?," *Space Sci.Rev.* **100** (2002) 195–206, `arXiv:astro-ph/0110211`.

[14] V. Sahni and Y. Shtanov, "Braneworld models of dark energy," *JCAP* **0311** (2003) 014, `arXiv:astro-ph/0202346v3`.

[15] E. P. Verlinde, "Emergent Gravity and the Dark Universe," *SciPost Phys.* **2** (2017) 16, `arXiv:1611.02269 [hep-th]`.

[16] B.S. Haridasu, V.V. Luković, R. D'Agostino, and N. Vittorio, "Strong evidence for an accelerating Universe," *Astron. Astrophys.* **600** (2017) no. 2015, L1, `arXiv:1702.08244 [astro-ph]`.

[17] A. Kamenshchik, U. Moschella, and V. Pasquier, "An alternative to quintessence," *Phys. Lett. Sect. B* **511** (2001) 265–268, `arXiv:gr-qc/0103004`.

[18] M. C. Bento, O. Bertolami, and A. A. Sen, "Generalized Chaplygin gas, accelerated expansion, and dark-energy-matter unification," *Phys. Rev. D* **66** (2002) 43507, `arXiv:gr-qc/0202064`.

[19] N. Bilic, "Unification of dark matter and dark energy: the inhomogeneous Chaplygin gas," *Phys. Lett. B* **535** (2002) 17–21, `arXiv:astro-ph/0111325`.

[20] H.B. Sandvik, M. Tegmark, M. Zaldarriaga and I. Waga, "The End of Unified Dark matter?," *Phys. Rev. D* **69** (2004) 123524, `arXiv:astro-ph/0212114v2`.

[21] J. Abha Dev, Alcaniz and D. Jain, "Cosmological consequences of a chaplygin gas dark energy," *Phys. Rev. D* **67** (2003) 023515, `arXiv:astro-ph/0209379`.

[22] D. J. Alcaniz, J.S. and A. Dev, "High-redshift objects and the generalized chaplygin gas," *Phys. Rev. D* **67** (2003) 043514, `arXiv:astro-ph/0210476`.

[23] V. Gorini, A. Kamenshchik, and U. Moschella, "Can the Chaplygin gas be a plausible model for dark energy?," *Phys. Rev. D* **67** (2003) no. 6, 1–6, `arXiv:astro-ph/0209395`.

[24] M. Makler, S. Q. De Oliveira, and I. Waga, "Constraints on the generalized Chaplygin gas from supernovae observations," *Phys. Lett. Sect. B Nucl. Elem. Part. High-Energy Phys.* **555** (2003) 1–6, `arXiv:astro-ph/0209486`.

[25] V. Gorini, A. Y. Kamenshchik, U. Moschella, O. F. Piattella, and A. A. Starobinsky, "Gauge-invariant analysis of perturbations in Chaplygin gas unified models of dark matter and dark energy," *J. Cosmol. Astropart. Phys.* **2008** (2008) 016, `arXiv:0711.4242 [astro-ph]`.

[26] V. Gorini, A. Y. Kamenshchik, U. Moschella, O. F. Piattella, and A. A. Starobinsky, "More about the Tolman-Oppenheimer-Volkoff equations for the generalized Chaplygin gas," *Phys. Rev. D - Part. Fields, Gravit. Cosmol.* **80** (2009) 1–8, `arXiv:0909.0866 [astro-ph]`.

[27] C-G. Park, J-C. Hwang, J. Park, and H. Noh, "Observational constraints on a unified dark matter and dark energy model based on generalized chaplygin gas," *Phys. Rev. D* **81** (2010) 063532, `arXiv:0910.4202 [astro-ph]`.

[28] A. A. El-Zant, "Unified dark matter: Constraints from galaxies and clusters," *Mon. Not. R. Astron. Soc.* **453** (2015) 2250–2258, `arXiv:1507.07369 [astro-ph]`.

[29] P. Bhar, M. Govender, and R. Sharma, "Modeling Anisotropic Stars Obeying Chaplygin Equation of State," (2016) 1–14, `arXiv:1605.01274v1 [gr-qc]`.

[30] R. Aurich and S. Lustig, "On the compatibility of the Chaplygin gas cosmology with recent cosmological data," `arXiv:1704.01749 [astro-ph]`.

[31] S. Saha, S. Ghosh, and S. Gangopadhyay, "Interacting Chaplygin gas revisited," `arXiv:1701.01021 [gen. physics]`.

[32] R. F. vom Marttens, L. Casarini, W. Zimdahl, W. S. Hipólito-Ricaldi, and D. F. Mota, "Does a generalized Chaplygin gas correctly describe the cosmological dark sector?," `arXiv:1702.00651 [astro-ph]`.

[33] S. Chaplygin, "On gas jets," *Sci. Ann. Imp. Univ. Mowcow* **21** (1904) .